Mode-Coupling Induced Crosstalk Optimization in a Graded-Index Six-Mode Fiber

Tianfeng Zhao, Feng Wen, *Member, IEEE*, Baojian Wu, Bo Xu, and Kun Qiu

***Abstract*—We thoughtfully investigate the feasibility of reducing the mode-coupling caused crosstalk by optimizing the practical parameters of the few-mode fiber (FMF), based on the linear coupling theory. According to our simulation results, the low crosstalk FMF could be achieved with the small fiber core, the low refractive-index (RI) related parameters, the long operating-wavelength and the low core-eccentricity (CE). Moreover, the transmission behaviors over the fixed coupling and the random coupling scenarios are also discussed. The power distribution and the signal to interference plus noise ratio (SINR) evolutions along FMF reveal the impacts from the mode-coupling induced crosstalk in the spatial division multiplexing (SDM) transmission system. The random nature of the mode coupling suggesting the turbulent results are obtained in our simulation, confirmed the observation in the SDM test. And only a 1.23 dB SINR degradation of 16-QAM signals can be realized after 100 km transmission with the optimized CE of lower than 4×10^{-3}.**

***Index Terms*—Spatial division multiplexing (SDM), crosstalk (XT), mode coupling, few-mode fiber (FMF).**

I. Introduction

THE transmission data-rate of the commercial optical communication networks based on standard single-mode fibers (SSMFs) is now approaching their Shannon limit, which extremely stimulates the novel technology developments enabling increasing the system capacity or the spectral efficiency [1]. The spatial-division multiplexing (SDM) technology employing few-mode fibers (FMFs), multi-core fibers (MCFs), or the combination structure multi-core few-mode fibers (MC-FMFs) is a promising candidate to increase significantly the spectral efficiency of the transmission systems. Among them, the FMF could be considered as a special fiber developed from the multi-mode fiber (MMF), which has been commercially utilized in the short-distance optical transmission over several decades [2]–[4], by reducing the core diameter to limit the number of the guided modes. Moreover, the SDM technology based on FMFs, MCFs or MC-FMFs has performed their huge capacity through the experimental investigations, e.g., the records 456 bit/s/Hz [5], 1099.9 bit/s/Hz [6] demonstrated in such system thanks to the great spatial-utilization in a single fiber. However, in the SDM system the crosstalk-induced signal distortion severely degraded the transmission performance. As the fiber optimization of MCFs focuses on the core pitch to reduce the inter-core crosstalk [7], the design of the FMF channel no matter from the single-core fiber or the MC fiber structure is to reduce the crosstalk from the neighboring spatial-modes. In this paper, we focus on the fiber optimization to directly reduce this mode-coupling-induced crosstalk during the signal propagating.

Intensive investigations have been carried out on the design of the FMF [8]–[10] as well as the transmission performance over the SDM channels [11]–[13]. Multiple effects, e.g., the transmission attenuation, the mode coupling, the differential mode group delay (DMGD) and even the Kerr nonlinearity have been taken into account in the fiber design [8], [10], [14], [15]. Among those factors who severely degrade the signal quality, the mode coupling between optical light with different modes, especially its random coupling behavior is to define the power distribution as well as the noise accumulation along the FMF channel. In the transmission of the order of hundreds of kilometers, the SDM system with the weakly coupled FMF has the potential to remove the complex multi-input multi-output (MIMO) module [14]. Therefore, the FMF design in the view of the weak mode-coupling is the key to perform a high-capacity, low digital-signal-processing (DSP) complexity SDM transmission system. Several theoretical models have been proposed to investigate the random coupling behavior in the FMF, i.e., the semi-analytical model for a linear coupling FMF [16], the matrix model of multimode fibers in the strong coupling region [17]. In those models, the coupling characters induced by the parameter "coupling coefficient" were considered, and the crosstalk (XT) as the consequent of the mode coupling were investigated. In the previous design works on the weakly coupled FMF [18]–[20], the coupling characteristic is considered as the function of the effective refractive-index (RI) difference Δn_{eff} between spatial-modes. For a weakly coupled FMF, the Δn_{eff} should be larger than 1×10^{-3} [18]. Although this parameter could be used to identify the coupling characteristics of FMFs, the more direct connection between the real fiber parameters, e.g., the fiber core dimension, the RI distribution and the core offset on the signal transmission performance is also important to the fiber design, that is well discussed in this work.

In this paper, we build a bridge between the XT strength and the real FMF parameters based on the perturbation method of the linear coupling theory. Moreover, we use the power distribution

Manuscript received 10 February 2022; revised 22 May 2022; accepted 27 June 2022. Date of publication 30 June 2022; date of current version 8 July 2022. This work was supported by the National Key R&D Program of China under Grant 2018YFB1801001. *(Corresponding author: Feng Wen.)*

The authors are with the Key Lab of Optical Fiber Sensing and Communication Networks, Ministry of Education, School of Information and Communication Engineering, University of Electronic Science and Technology of China, Chengdu 611731, China (e-mail: m18242105581@163.com; fengwen@uestc.edu.cn; bjwu@uestc.edu.cn; xubo@uestc.edu.cn; kqiu@uestc.edu.cn).

Digital Object Identifier 10.1109/JPHOT.2022.3187411

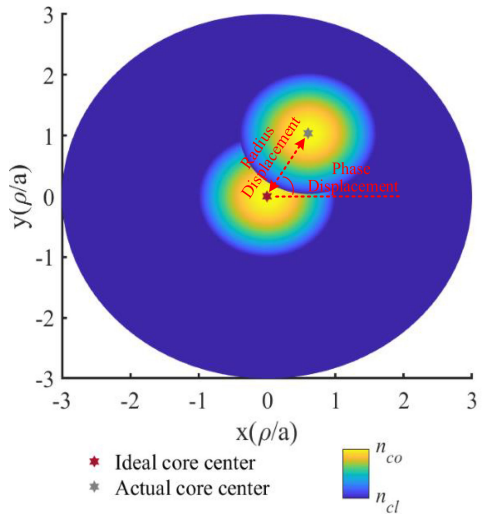

Fig. 1. Fiber RI profiles of ideal and actual cores.

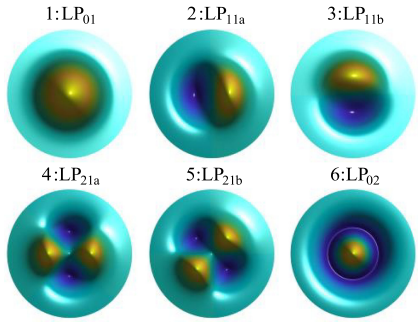

Fig. 2. Field distributions of the modes 1 to 6.

and the signal quality to quantify the distortion from the mode coupling in the FMF-based transmission system. The rest of the paper is organized as follows: in Section II, we introduce the theoretical model for the considered FMF, and the connection between the mode coupling and the real fiber parameters; in Section III, we thoughtfully investigate the dependence of the XT strength on the fiber parameters, i.e., the CE, the core radius, the relative RI difference, the cladding RI and the operating wavelength, which helps to locate the optimized values to reduce the distortion from the mode coupling; in Section IV, we propagate a 16-level quadrature amplitude modulation (16-QAM) signal over a 100km-lengh FMF to quantify the influence from the mode coupling in term of the power distribution and the signal to interference plus noise ratio (SINR) for both the fixed coupling and the random coupling scenarios; and finally, in Section V, we draw the conclusions of our study.

II. Fiber Parameters in the Mode Coupling

We considered a graded-index six-mode fiber (GI-6MF) channel, stimulating the LP_{01}, LP_{11a}, LP_{11b}, LP_{21a}, LP_{21b} and LP_{02} modes, corresponding to the mode number of 1 to 6 in the paper, and its standard RI profile (see ideal core case) depicted in Fig. 1 has been also defined in (1):

$$n(\rho) = \begin{cases} n_{co} \cdot [1 - \Delta \cdot (\rho/a)^{\alpha}], & |\rho| < a \\ n_{cl}, & |\rho| \geq a \end{cases} \quad (1)$$

where a is the fiber core radius, n_{co} and n_{cl} are the RIs of the core center and the cladding, α is the core shape parameter and Δ is the relative RI difference. The optical field E(x,y,z,t) stimulated in the six-mode fiber can be expressed in (2) as the linear combination of all guided optical modes:

$$\mathrm{E}(x,y,z,t) = \sum_{m} A_m(z,t)\mathrm{E}_m(x,y)e^{j(\omega t - \beta_m z)} \quad (2)$$

where m is the mode index, in our case $m = 1{\sim}6$; $A_m(z,t)$ is the slowly varying mode-filed envelope along the fiber longitudinal-coordinate z; β_m is the propagation constant at the frequency ω; $\mathrm{E}_m(x,y)$ is the electric field distribution in the fiber cross section, and the distributions corresponding to the mode 1 to 6 are also depicted in Fig. 2. According to the mode coupling model in [16], the imperfect fabrication process and the mechanical stress applied on the FMF inevitably produce continuous perturbations on the core-cladding boundary along the FMF. And the FMF is approximately discretized into segments along the propagation axis. Thus, in each segment, there will be a core mismatching along the FMF, and consequently inducing the deviation of the RI distribution from the ideal center to the slight shifting of the actual core, named CE, see the illustration in Fig. 1. This RI inhomogeneity production (i.e., $\Delta n(x,y,z)$), considered to be generated only by CE in this paper, causes the power coupling between the propagating mode and its neighboring modes. According to the mode coupling theory, this behavior can be expressed by the following equations [16]:

$$\partial_z A_m(z,t) = -\mathrm{j}\sum_{n} C_{mn}(z)A_n(z,t)\mathrm{e}^{\mathrm{j}(\beta_m - \beta_n)z} \quad (3)$$

where C_{mn} is the coupling coefficient between mode m and n, its expression given in (4) confirms the coupling strength is a function of the RI perturbation $\Delta n(x,y,z)$. Following the (3), the coupling behavior is also sensitive to the mismatching of the propagation constants, see β_m-β_n in the exponential function, which indicates the coupling diversity happened between different optical modes.

$$C_{mn}(z) = \frac{\omega\varepsilon_0}{4}\int\int_{-\infty}^{+\infty}[\Delta n(x,y,z)]^2 \cdot \mathrm{E}_m^* \cdot \mathrm{E}_n dxdy \quad (4)$$

As we can see in Fig. 1, the CE includes two elements, i.e., the radius displacement (RD) between ideal and actual cores and the phase displacement (PD) away from the reference direction, just as the radius and angular in the polar coordinate system. Therefore, the RI perturbation Δn as well as the coupling coefficient C_{mn} are also dependent on these two elements when CE happened in the FMF.

In what follows, we investigate the CE parameters to influence the mode coupling in FMF. The discussion focuses on the coupling coefficient C_{mn} due to its importance in the mode coupling, see (3). We plotted the distribution of C_{mn} as a function of the normalized RD, which was defined by core displacement/core radius from 0 to 0.8 and the PD from 0 to 2π, see in Fig. 3.

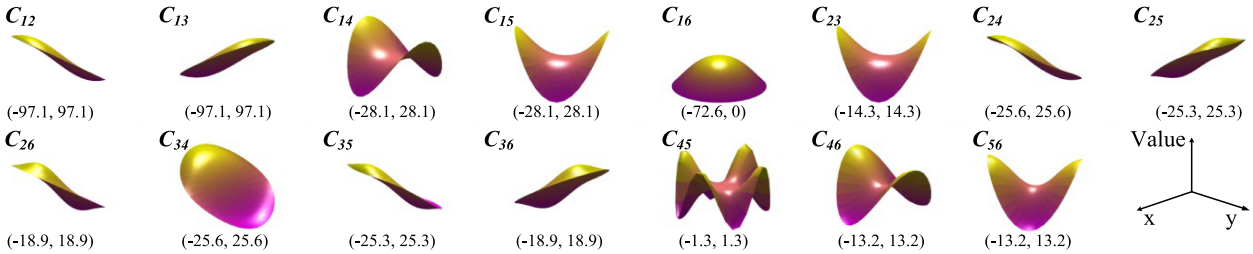

Fig. 3. C_{mn} profiles as a function of CE, minimum and maximum values given in (min, max) for each case.

The other FMF parameters were: the core radius $= 12$ μm, the cladding RI $n_{cl} = 1.443$, the relative RI difference $\Delta = 2.5 \times 10^{-3}$ at 1550 nm, and the core shape parameter $\alpha = 2.33$. The parameter values were the same level to a real GI-6MF produced by YOFC [21]. For a 6-mode channel system, the total number of coupling coefficients should be 30, here only given 15 due to the same distribution obtained from C_{mn} and C_{nm}. According to (4), the shape of the coupling coefficient is relative to the field distribution. For example, the mode fields of LP_{11a} and LP_{11b} are rotated by 90°, so that the rotation between C_{12} and C_{13} is also 90°. We could observe the similar behavior in [16] as well. Therefore, based on the results from (4) and Fig. 3, we can find out these parameters, i.e., the radius and phase displacements, the core size, the RI related parameters and the operating wavelength as the key elements to define the mode coupling behavior in FMF, which implies the possibility to reduce the coupling strength by optimizing fibers.

III. Parameter Optimization for Low Crosstalk

In the following, we investigate the dependency of the crosstalk caused by the mode coupling on various FMF parameters. The $\mathrm{XT}_m = \Sigma_{v \neq m}(P_v/P_m)$ is defined as the crosstalk strength of mode m, where P_v is the power of mode v after single coupling when only the mode m is launched. When we calculated the XT_m results, only one parameter was changed to give a clear dependence between the crosstalk strength and the single fiber parameter. Fig. 4 depicts the calculated XT_m curves of each mode for different FMF parameters, i.e., the normalized RD, the core radius a, the cladding RI n_{cl}, the relative RI difference Δ, the operating wavelength λ and the core shape parameter α. To give a fair comparison, we monitored the normalized frequency V throughout to guarantee the FMF considered supporting six modes at 1550nm. We have also investigated the two cases with or without degenerated modes. When the degenerated modes taken into account, i.e., LP_{11a} and LP_{11b} channels or LP_{21a} and LP_{21b} channels delivering different information, the higher system rate is naturally expected, but the more crosstalk is also observed due to mismatching condition in (3). All the XT_m results are shown in Fig. 4 and a part of rules are the same as those in our previous work [22].

When CE considered in FMF, the mode coupling introduces the energy flowing between two different modes, quantified by XT_m in Fig. 4(a) and (b). In the simulation we focused on the RD as the core parameter when CE happened, and the impact from PD was still considered through the mean-value operation from 0 to 2π for each coupled field $A_m(z,t)$. Increasing the value of RD, implying the severe core displacement happened in fibers leads to the higher crosstalk, more than 60 dB stronger crosstalk obtained when the normalized RD increased by three orders of magnitude. Moreover, when the degenerated modes treated as the independent channels, about 40 dB stronger crosstalk is obtained between these modes compared to the non-degenerated modes, see in Fig. 4(b). We also can see that the same XT-level achieved within the degenerated modes, i.e., LP_{11a} and LP_{11b}, LP_{21a} and LP_{21b}, confirms the major noise coming from the energy coupling among the intra-group instead of the inter-group modes.

Then, the impact from the core radius a is discussed in Fig. 4(c) and (d). The core radius influences the electric field distribution E_m in the fiber cross section and consequently the coupling coefficient C_{mn}, see (4). The similar curves obtained in both cases with non-degenerated and degenerated modes. Much higher crosstalk was achieved by degenerated modes LP_{11a} and LP_{11b}, LP_{21a} and LP_{21b} in Fig. 4(d) when the normalized RD $= 3 \times 10^{-3}$. We also could locate the minimum $\mathrm{XT}_m = -81$ dB and -79 dB around $a = 10.5$ for both LP_{21} and LP_{02} in Fig. 4(c) suggesting the importance of the optimization procedure.

The influence from the RI related parameters is investigated in Fig. 4(e)–(j), where the relative RI difference Δ, the cladding RI n_{cl}, the core parameter α and the core shape parameter α considered. These parameters are directly connected to the RI profile of FMF, naturally defining the RI perturbation Δn and the coupling coefficient C_{mn} as well, see (4). More specifically, the reductions of Δ and n_{cl} reduce the Δn, so that the coupling crosstalk is suppressed with them, depicted in subfigure (e) to (h). The slope of XT_m curves for n_{cl} is lower than the case of Δ due to the less impact from n_{cl} on Δn. All simulation results confirm that the smaller values of Δ and n_{cl} introduces the less mode-coupling crosstalk. In addition, the XT response on the increase of the α is different from the other parameters. As depicted in Fig. 4(i), only considering the non-degenerated modes, there are peaks observed for XT_1 and XT_2 when α equals to around 1.7, and the increase of XT_3 and XT_4 gradually saturates with α. In the case of the degenerated modes, the coupling between degenerate modes makes XT of these modes increase significantly with α, as shown in Fig. 4(j).

The last parameter we discussed is the operating wavelength λ which is important to the operation of the wavelength division multiplexing (WDM) transmission system. The influence of the

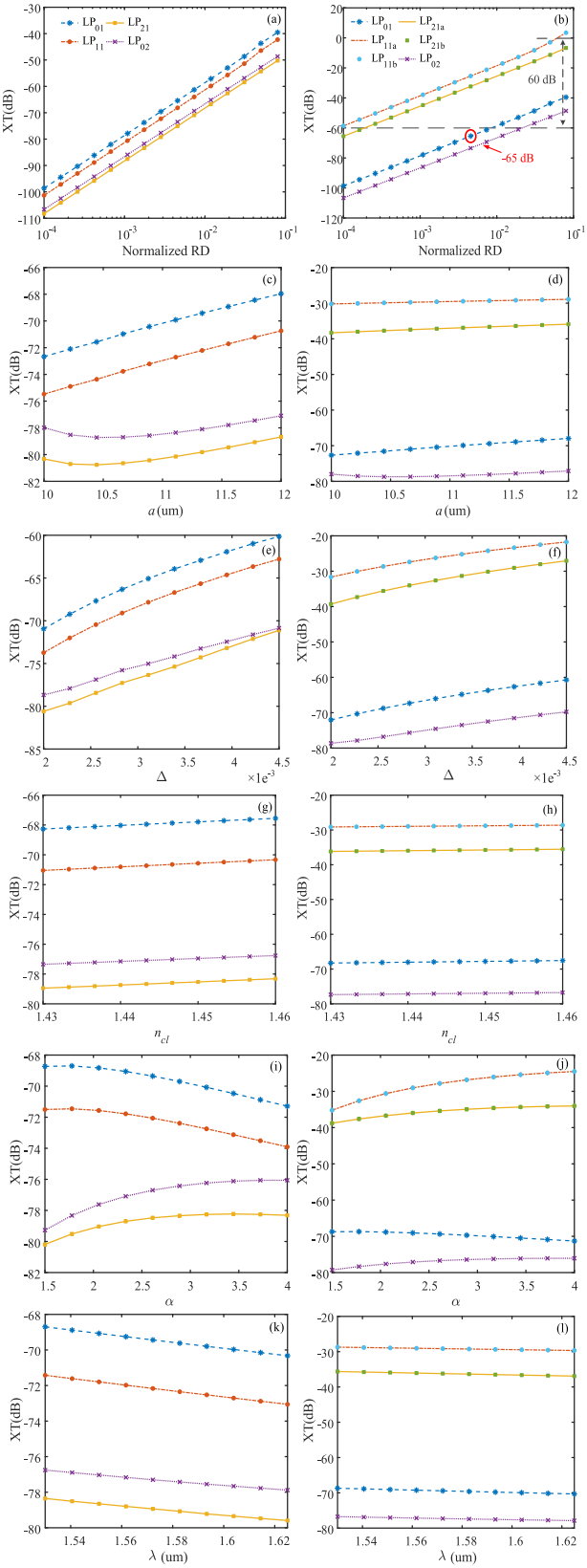

Fig. 4. XT_m results for normalized RD, core radius a, relative RI difference Δ, cladding RI n_{cl}, core shape parameter α and operating wavelength λ in non-degenerated modes considered case ((a), (c), (e), (g) (i) and (k)) and degenerated modes considered case ((b), (d), (f), (h) (j) and (l)), respectively.

operating wavelength comes from the angular frequency ω in (4). We calculated the whole C+L band and found out the less crosstalk obtained from the longer operating wavelength. However, the crosstalk diversity of WDM channels implies the independent training operations of the MIMO equalizer required for different operating wavelengths, increasing the cost of the system compensation for WDM over SDM channels.

To sum up, we could reduce the crosstalk strength caused by the mode coupling through optimizing the parameters of FMF, including smaller RD, core radius, cladding RI, relative RI difference and longer operating wavelength. And we iterate the FMF parameters with fixed normalized RD of 3×10^{-3} to find the optimal parameter combination corresponding to the minimum XT of each mode. On the whole, the optimal parameter combination was a = 12 μm, $\Delta = 2.28 \times 10^{-3}$, $n_{cl} = 1.43$, α = 1.2 and λ = 1582.78 nm, and the corresponding crosstalk are $XT_1 = -77.90$ dB, $XT_2 = -39.57$ dB, $XT_3 = -39.57$ dB, $XT_4 = -44.67$ dB, $XT_5 = -44.67$ dB and $XT_6 = -84.08$ dB. In addition, the less crosstalk was indeed obtained when the non-degenerated modes weren't taken into account, but the transmission capacity of the SDM system also significantly reduced. Therefore, the optimization for FMF becomes extremally important for this intensively multiplexing technology.

IV. Transmission Investigation Over a 100 km Six-Mode Fiber

In this section, we evaluate the transmission performance of GI-6MF combined with the crosstalk investigation in Section III, including the degenerated channels. In the simulation, the mode coupling was not only considered at a certain point as we discussed in the previous section, but also cascaded calculation through the whole fiber by the step of the coupling length, this accumulation operation also used in the other FMF models [17], [23], [24]. Mode coupling only happened at the beginning of each coupling length through the matrix U_n, see the "coupling length" labelled in Fig. 5. In the following simulation, we set 500m as the coupling length as [11], [23].

Before the transmission, we firstly mapped six independent sets of pseudo-random binary sequence (PRBS) data with the length of $2^{31}-1$ to 16-QAM signals for six modes, as shown in Fig. 5. After setting the signal power of each mode as 0dBm and the initial signal-to-noise ratio (SNR) as 25 dB, the data of six channels were injected into the ideal mode multiplexer and propagated in the six-mode fiber. To focus on the impact from the mode coupling, we only considered the crosstalk from all kinds of spatial modes as the noise source to reveal the signal evolution within the FMF. We defined ${A_m}^{n-1}(z,t)$ as the slowly-varying mode-field envelope of mode m before the nth coupling, and ${A_m}^{n-1}(z,t)$ of all six modes combined into a column vector $A^{n-1}(z,t) = [{A_1}^{n-1}, {A_2}^{n-1}, \ldots, {A_6}^{n-1}]^T$. For the nth mode coupling, we set $A^n = U^n \cdot A^{n-1}$ as the output column vector, where U^n is the unitary coupling matrix solved from (3) with the Runge-Kutta-Fehlberg (RK45) method. According to (3), we can list six differential equations to solve the coupled A_m ($m = 1 \sim 6$) with the known C_{mn} and the preset input A_m vector before coupling.

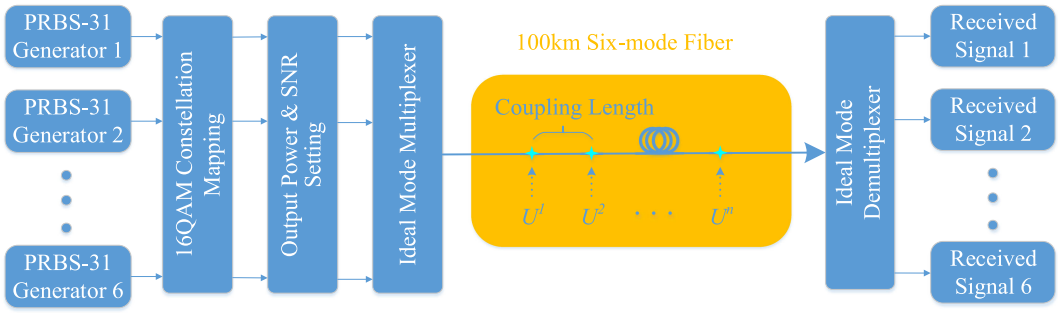

Fig. 5. Simulation setup for the few-mode transmission over a 100 km six-mode fiber.

TABLE I
THE FIXED COUPLING MATRIX U^N WITH THE CE OF THE NORMALIZED RD $= 4 \times 10^{-3}$

	LP_{01}	LP_{11a}	LP_{11b}	LP_{21a}	LP_{21b}	LP_{02}
LP_{01}	0.999999	3.83e^{-4}	3.70e^{-4}	1.31e^{-5}	-2.68e^{-5}	4.81e^{-5}
LP_{11a}	-3.83e^{-4}	0.999956	9.41e^{-3}j	4.92e^{-6}j	5.42e^{-6}j	3.62e^{-6}j
LP_{11b}	-3.70e^{-4}	-9.41e^{-3}j	0.999956	-4.40e^{-6}j	5.25e^{-6}j	3.54e^{-6}j
LP_{21a}	-1.31e^{-5}	4.92e^{-6}j	-4.40e^{-6}j	0.999990	-4.42e^{-3}j	3.83e-6j
LP_{21b}	2.68e^{-5}	5.42e^{-6}j	5.25e^{-6}j	4.42e^{-3}j	0.999990	-7.30e^{-6}j
LP_{02}	-4.81e^{-5}	3.62e^{-6}j	3.54e^{-6}j	3.83e^{-6}j	-7.30e^{-6}j	0.999999

Then, in order to obtain the coupling matrix, we preset the input A_m vector as a one-hot vector. For example, when we set the kth value of input A_m to 1 and the others to 0, the output A_m vector is set as the kth column of the coupling matrix, representing the energy transformed for the kth mode to other modes in the coupling. In addition, the fiber parameters were the same as mentioned in Section II. At the end of the 100 km-FMF, six groups of received data were separated through an ideal mode demultiplexer, and launched into the receiver to evaluate the signal quality. The rare data without optical MIMO equalization were directly used to calculate the SINR results, which contains the valued distortion information from the mode coupling. We considered two transmission scenarios: propagating through the FMF with the same, fixed coupling matrix, or the randomly generated matrices. The first scenario gives the clear impact from the mode coupling, and the later one is closer to the real implementation.

For the first scenario, we calculated the coupling matrix U^n for all six modes, given in Table I. In the simulation, the normalized RD value was chosen as 4×10^{-3}, and the corresponding crosstalk for six-modes were $XT_1 = -65$ dB, $XT_2 = -25$ dB, $XT_3 = -25$ dB, $XT_4 = -32$ dB, $XT_5 = -32$ dB and $XT_6 = -73$ dB confirming the weakly coupling FMF considered in the transmission, also seen in Fig. 4(b). From the coupling matrix, we could locate the stronger crosstalk happened between two degenerated modes, as we discussed in previous section. For the fixed coupling case, all of the coupling matrices are the same through the whole FMF. We calculated and depicted the SINR and signal power properties versus the transmission distance in Fig. 6(a) and (b), with a fixed coupling matrix U^n, which contains total 200 matrices through the 100 km fiber. In Fig. 6(a), the SINR result of each mode decreases with the transmission distance from 0 to 100 km with different speeds. And the larger the variation of the power, representing the crosstalk strength of a certain mode in Fig. 4(b), the faster the SINR of this mode decreases. According to Fig. 6(b), as a result of mode coupling, the power of each mode fluctuates periodically during the transmission. And even the power of LP_{11a} and LP_{11b} returns to the initially launched value, around 0 dBm, at near 80 km, the SINR of these two modes is still decreasing, so that the signal quality does not depend on the power level of the spatial modes, but on the power exchange level, i.e., XT_m of each mode during the propagating. We simulated the SINR degradation with XT_1 strength under the same transmission distance of 100 km and depicted the results in Fig. 6(c). The considered XT_1 is -49, -65, -82 and -99 dB, corresponds to the normalized RD values of 3×10^{-2}, 4×10^{-3}, 6×10^{-4} and 1×10^{-4}. We can find that the weaker XT is helpful to suppress the signal deterioration after a period of transmission. In Fig. 6(d), we plotted the SINR-transmission distance curves of LP_{01} as an example, with the XT_1 strength of -49, -65 and -82 dB, respectively. And the constellation results at the same 40 km of each case are given for comparison. Consistent with the results in [16], the increase of coupling strength results the higher of XT accumulation with the transmission distance. At the same time, the clear constellation with less CE impact implies the

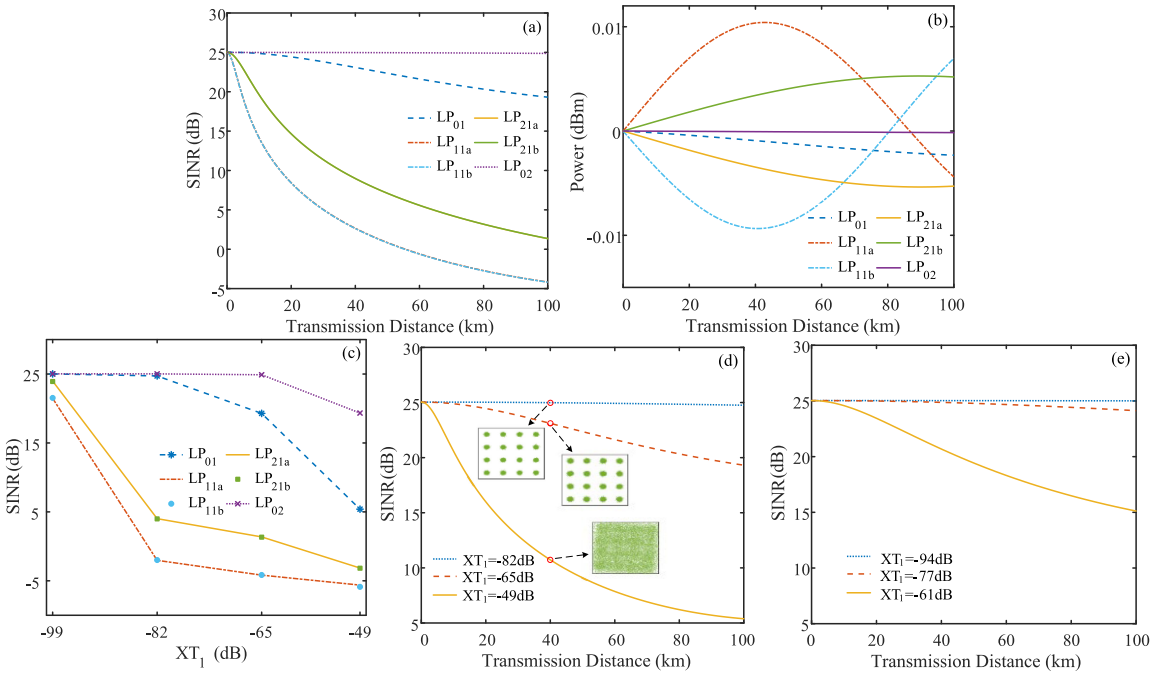

Fig. 6. Relationships between transmission distance and (a) SINR, (b) signal power with fixed coupling matrix. (c) SINR curves with different XT_1 under 100 km transmission. (d) SINR curves during transmission with XT_1 of -82 dB, -65 dB and -49 dB for GI-6MF. (e) SINR curves during transmission with XT_1 of -94 dB, -77 dB and -61 dB for GI-3MF.

significant reduction of the complex from MIMO compensation algorithm, proving the importance of the parameter optimization in Section III. Furthermore, in order to prove the conclusion is also applicable to other weakly coupled GI-FMFs, we also tested the signal quality with the transmission distance under different XT_1 in GI-3MF, results depicted in Fig. 6(e). The considered parameters of GI-3MF were the same as the GI-6MF, except the core radius of 7.5 μm. And the normalized RDs corresponding to XT_1 in Fig. 6(e) are consistent with them in Fig. 6(d). Due to the less modes stimulated in the GI-3MF, the generated XT with the same RD is also reduced. Although the strength of XT is different between GI-6MF and GI-3MF, the dependency of the signal quality on the transmission distance and the XT is the same. Therefore, the optimized conclusion could be used to guide the fiber design and evaluate the transmission performance for the weakly coupled GI-FMFs.

Moreover, the second scenario with the randomly generated coupling matrices is investigated. The random-coupling nature of the FMF channel induced the oscillatory data-waveform and consequently the fluctuations on the test of the signal quality, the time-dependent channel already observed in [25]–[27]. In the simulation, we not only randomly generated 200 coupling matrices along the 100 km FMF representing the accumulated impact from the mode coupling, but also tested the whole transmission system over 60 times by randomly allocating the coupling strength for each time, which introduced the time-dependent channel property of the FMF-based transmission system. The normalized RD value was selected within the range of $4 \times 10^{-3} \pm 3 \times 10^{-4}$, with a uniform distribution to randomly generate the coupling matrix. In this range, the weakly coupling channel was maintained to each time. For each coupling, the value of RD is randomly located within this range to figure out the corresponding coupling matrix. When the RD changes, the distributions of Δn and C_{mn} in the cross section of the FMF change accordingly, as expressed in (4) and shown in Figs. 1 and 3. Thus, the distributions of Δn and C_{mn} for each coupling are random and independent. In Fig. 7(a), we plotted the mean SINR values of each mode after propagating through 100 km FMF with random coupling. Similar behavior was observed between the random coupling case from Fig. 7(a) and the fixed coupling case in Fig. 6(a), due to the same RD mean-value used in both scenarios. And the corresponding mean power vs. transmission distance curves were plotted in Fig. 7(b). A clear turbulence on both SINR and power results are observed coming from the random coupling allocation. The detail variations from the 60 independent tests were depicted in Fig. 7(c) and (d). These results correspond to LP_{21a} mode at 54.5 km, see the yellow-star mark in Fig. 7(a). Because of the random coupling happened for each test-time, the calculated SINR and the optical power were different from the rare data. This demonstrates the real-time signal quality is fluctuated with the oscillatory data-waveform, just as the observation in the experiment. We have also given the relationship between SINR and XT_1 in Fig. 7(e) with a fixed transmission distance. The simulation was also considered the random coupling matrices and the RD values correspond to the considered XT_1 from large to small are uniformly distributed with the mean values of 3×10^{-2}, 4×10^{-3}, 6×10^{-4} and 1×10^{-4} and the variance of 3×10^{-8}. In Fig. 7(f), we have depicted the mean SINR values of LP_{01} with different RDs, with the same distribution of them in Fig. 7(e). It's obvious from Fig. 7(e) and (f) that the larger mean RD, the greater SINR decreases, which confirms the conclusion in Fig. 6(c)

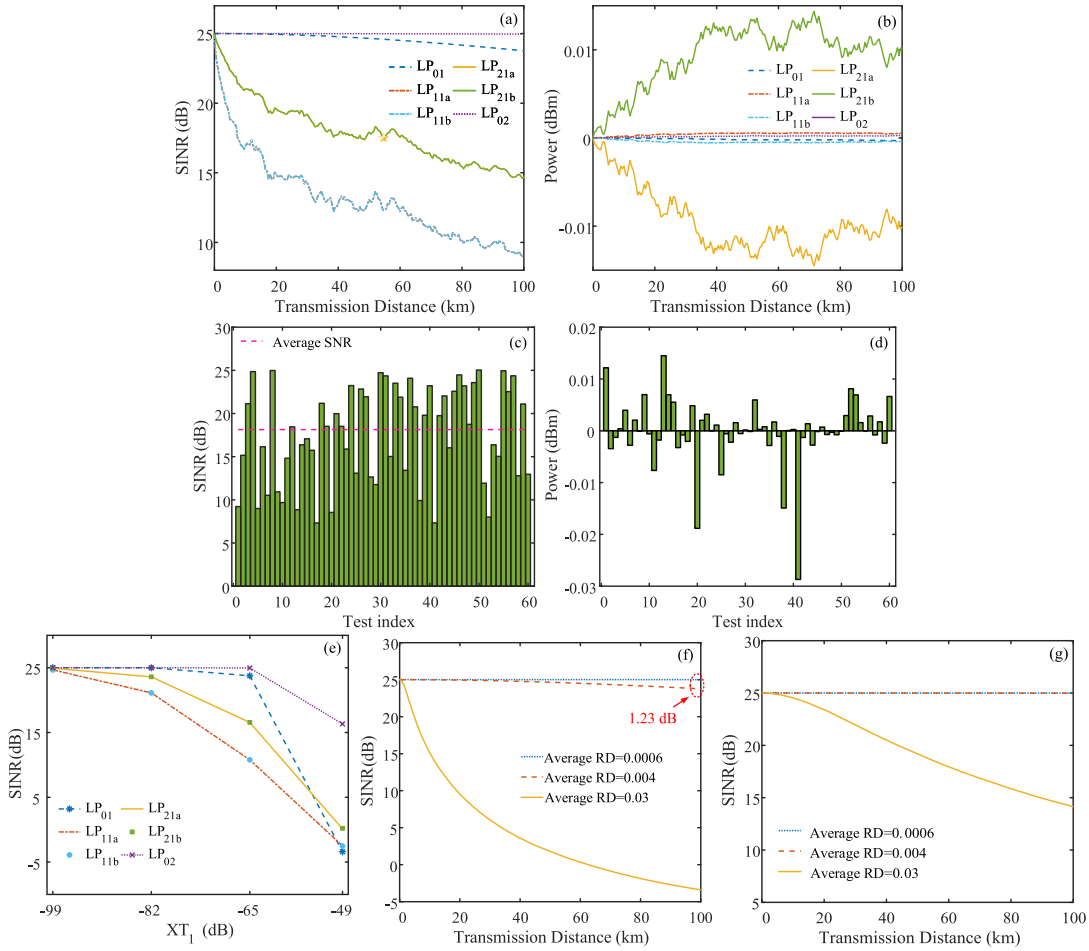

Fig. 7. Relationships between transmission distance and (a) SINR, (b) signal power with random coupling matrix, (c) SINR and (d) power distribution of the 60 independent simulations for the yellow star of LP_{21b}, (e) SINR curves with different XT_1 under 100 km transmission in random scenario. SINR curves of LP_{01} with the mean RD of 3×10^{-2}, 4×10^{-3} and 6×10^{-4} for (f) GI-6MF and (g) GI-3MF.

and (d). Furthermore, we can see that once the RD is less than 4×10^{-3}, the degradation of SINR for LP_{01} mode after 100 km transmission can be less than 1.23 dB. Then, in Fig. 7(g), we also give the degradation of SINR with transmission distance at different average RD in GI-3MF. And the rules demonstrated are consistent with Fig. 6(e). According to the results from both scenarios, reducing the mode coupling through optimizing the FMF parameters is feasible to improve the practical SDM transmission performance.

In above transmission, we neglect other inherent distortion generated in the FMF channel (e.g., attenuation, dispersion and Kerr nonlinearity) that would further degrade the signal quality in practice, but mainly focus on the characteristics of mode coupling induced crosstalk, which shapes the transmission response of FMF and is significant for transmission performance evaluation.

V. Conclusion

Firstly, we discussed the possibility of reducing the crosstalk strength by optimizing the FMF parameters based on the linear coupling theory. Then, we simulated the properties of various fiber parameters on the mode-coupling caused crosstalk, and the reduction of XT-level in the graded-index six-mode fiber could be achieved up to 60 dB by properly designing the core size, RI values, RD and operating wavelength. According to the transmission simulation results with the fixed or random coupling matrices, we find that the power value can't be used to monitor the signal quality, which is an oscillatory function of the transmission distance. The SINR results of the transmitted signals is more sensitive to the crosstalk strength, confirming the importance of the optimization procedure. And we could achieve only a 1.23 dB SINR degradation with the optimized RD less than 4×10^{-3} after the transmission of the 100 km GI-6MF.

Acknowledgment

The authors thanks the high-performance simulation from Rampur-Hybrid Machine powered by Marolabs Company.

References

[1] N. Hanzawa *et al.*, "Demonstration of mode-division multiplexing transmission over 10 km two-mode fiber with mode coupler," in *Proc. OSA Opt. Fiber Commun. Conf.*, 2011, Art. no. OWA4.

[2] A. Inoue and Y. Koike, "Low-noise graded-index plastic optical fiber for significantly stable and robust data transmission," *J. Lightw. Technol.*, vol. 36, no. 24, pp. 5887–5892, Dec. 2018.

[3] A. Simović *et al.*, "Investigation of bandwidth in multimode graded-index plastic optical fibers," *Opt. Exp.*, vol. 29, no. 19, pp. 29587–29594, 2021.
[4] S. Savović and A. Djordjevich, "New method for calculating the coupling coefficient in graded index optical fibers," *Opt. Laser Technol.*, vol. 101, pp. 223–226, 2018.
[5] K. Igarashi *et al.*, "Ultra-dense spatial-division-multiplexed optical fiber transmission over 6-mode 19-core fibers," *Opt. Exp.*, vol. 24, no. 10, pp. 10 213–10 231, 2016.
[6] D. Soma *et al.*, "10.16-peta-b/s dense SDM/WDM transmission over 6-mode 19-core fiber across the C+L band," *J. Lightw. Technol.*, vol. 36, no. 6, pp. 1362–1368, Mar. 2018.
[7] K. Saitoh, "Multi-core fiber technology for SDM: Coupling mechanisms and design," *J. Lightw. Technol.*, vol. 40, no. 5, pp. 1527–1543, Mar. 2022.
[8] F. M. Ferreira, D. Fonseca, and H. J. A. da Silva, "Design of few-mode fibers with M-modes and low differential mode delay," *J. Lightw. Technol.*, vol. 32, no. 3, pp. 353–360, Feb. 2014.
[9] L. Ma, K. Tsujikawa, N. Hanzawa, S. Aozasa, S. Nozoe, and F. Yamamoto, "Design and fabrication of low loss hole-assisted few-mode fibers with consideration of surface imperfection of air holes," *J. Lightw. Technol.*, vol. 34, no. 22, pp. 5164–5169, Nov. 2016.
[10] H. Zhang, J. Zhao, Z. Yang, G. Peng, and Z. Di, "Low-DMGD, large-effective-area and low-bending-loss 12-LP-mode fiber for mode-division-multiplexing," *IEEE Photon. J.*, vol. 11, no. 4, Aug. 2019, Art. no. 7203808.
[11] T. Zhao *et al.*, "Noise analysis and MIMO equalization for a spatial-division multiplexing (SDM) transmission system," in *Proc. OSA Asia Commun. Photon. Conf.*, 2020, Art. no. M4A.234.
[12] K. Ho and J. M. Kahn, "Linear propagation effects in mode-division multiplexing systems," *J. Lightw. Technol.*, vol. 32, no. 4, pp. 614–628, Feb. 2014.
[13] W. S. Saif, A. M. Ragheb, T. A. Alshawi, and S. A. Alshebeili, "Optical performance monitoring in mode division multiplexed optical networks," *J. Lightw. Technol.*, vol. 39, no. 2, pp. 491–504, Jan. 2021.
[14] L. Shen *et al.*, "Design, fabrication, measurement and MDM transmission of a novel weakly-coupled ultra low loss FMF," in *Proc. OSA Opt. Fiber Commun. Conf.*, 2018, Art. no. Th2A.24.
[15] J. Liu *et al.*, "Design and optimization of weakly-coupled few-mode fiber with low nonlinearity," *Chin. Opt. Lett.*, vol. 12, no. 3, 2014, Art. no. 030601.
[16] F. M. Ferreira, C. S. Costa, S. Sygletos, and A. D. Ellis, "Semi-analytical modelling of linear mode coupling in few-mode fibers," *J. Lightw. Technol.*, vol. 35, no. 18, pp. 4011–4022, Sep. 2017.
[17] K. Ho and J. M. Kahn, "Mode-dependent loss and gain: Statistics and effect on mode-division multiplexing," *Opt. Exp.*, vol. 19, no. 17, pp. 16 612–16 635, 2011.
[18] Z. He *et al.*, "Machine learning aided inverse design for few-mode fiber weak-coupling optimization," *Opt. Exp.*, vol. 28, no. 15, pp. 21668–21681, 2020.
[19] T. Hu *et al.*, "Weakly-coupled 4-mode step-index FMF and demonstration of IM/DD MDM transmission," *Opt. Exp.*, vol. 26, no. 7, pp. 8356–8363, 2018.
[20] S. Jiang *et al.*, "Design and characterization of ring-assisted few-mode fibers for weakly coupled mode-division multiplexing transmission," *J. Lightw. Technol.*, vol. 36, no. 23, pp. 5547–5555, Dec. 2018.
[21] "YOFC few-mode fiber parameters." [Online]. Available: http://en.yofc.com/view/2351.html
[22] T. Zhao *et al.*, "Crosstalk reduction for a graded-index six-mode fiber," in *Proc. OSA Front. Opt./Laser Sci.*, 2020.
[23] T. Zhao *et al.*, "Noise compensation for a nonlinear six-mode fiber channel through self-recycling training equalizer," in *Proc. OSA Optoelectron. Commun. Conf.*, 2021, Art. no. M3F.5.
[24] S. Ö. Arık, K. Ho, and J. M. Kahn, "Group delay management and multiinput multioutput signal processing in mode-division multiplexing systems," *J. Lightw. Technol.*, vol. 34, no. 11, pp. 2867–2880, Jun. 2016.
[25] M. Nakazawa, M. Yoshida, and T. Hirooka, "Measurement of mode coupling distribution along a few-mode fiber using a synchronous multi-channel OTDR," *Opt. Exp.*, vol. 22, no. 25, pp. 31299–31309, 2014.
[26] T. Zhao *et al.*, "Transmission performance and noise suppression in a two-mode fiber (TMF) channel," in *Proc. Int. Conf. U.K.–China Emerg. Technol.*, 2021, pp. 121–124.
[27] T. Zhao, F. Wen, and K. Qiu, "Spectral features with the temporal and spatial mode-coupling dynamic in a few-mode system," in *Proc. Photon. Electromagn. Res. Symp.*, 2022, pp. 547–552.